AIAA-2005-0993

JET NOISE SUPPRESSION WITH FAN FLOW DEFLECTORS IN REALISTIC-SHAPED NOZZLE

Dimitri Papamoschou *
Kimberley A. Nishi †
University of California, Irvine, California 92697-3975

This is an exploratory study of jet noise reduction using fan flow deflectors in a nozzle shaped like the exhaust of a separate-flow turbofan engine with bypass ratio 4.8. The deflectors directed the bypass plume downward and/or sideward relative to the core plume. Vane- and wedge-type deflectors were tested. The noise reduction achieved by the vane deflector was strong in the downward direction and moderate in the sideline direction. Wedge-type deflectors generated significant attenuation in both directions. Combination of vanes and wedge yielded the best results. The effective perceived noise level was suppressed by 5.5 dB in flyover mode and 3.8 dB in sideline mode.

Introduction

The increase in bypass ratio over the last three decades has resulted in a dramatic suppression in the jet noise of turbofan engines. Modern engines are so quiet that further reduction in noise becomes very challenging. The success of the high-bypass engine is offset by the increasing volume of aircraft operations. This creates more environmental and political pressures for quieter aircraft. Today the most successful technique for reducing jet noise from high-bypass engines involves the installation of chevron mixers on the exhaust nozzles [1]. However, the ever increasing need for quieter engines requires exploration of alternative techniques that could be used by themselves or in conjunction with existing methods.

The Fan Flow Deflection (FFD) technology is tailored for suppression of "large-scale" turbulent mixing noise from aircraft engines. Large-scale mixing noise is the dominant noise source in turbulent jets. The overarching principle of the FFD technology is reduction of the convective Mach number of turbulent eddies that generate intense downward and sideward sound radiation. In a coaxial separate-flow turbofan engine this is achieved by tilting in the general downward direction, by a few degrees, the bypass (secondary) plume relative to the core (primary) plume. Mean flow surveys show that the misalignment of the two flows causes a thick, low-speed secondary core on the underside of the high-speed primary flow, especially in the region near the end of the primary potential core which contains the strongest noise sources. The secondary core reduces the convective Mach number of primary eddies, thus hindering their ability to generate sound that travels to the downward acoustic far field [2]. Tilting of the bypass stream is possible by means of fixed or variable vanes installed near the exit of the bypass duct. Figure 1 depicts the general concept.

Earlier works on FFD used simple coaxial nozzles for the investigation of noise emission and mean flow field [2, 3]. This paper extends the previous work to nozzles shaped like the actual nozzle of a separate-flow turbofan engine. Also, it includes deflector configurations not covered by earlier studies. The treatment is exploratory. We report only on acoustic data and some preliminary flow visualizations. Aerodynamics and flow-field measurements will be covered by later papers.

Experimental Setup

Nozzle

The nozzle used in our experiments is a scaled-down version of the baseline separate-flow nozzle used in the Nozzle Acoustic Test Rig (NATR) of NASA Glenn Research Center [4]. The coordinates of the

*Professor, Associate Fellow AIAA
†Graduate student, Member AIAA

NATR nozzle were divided by a factor of eight to fit within the flow capacity of the UCI lab. Figure 2 plots the coordinates of the UCI nozzle. Stereolithography files were created and the nozzle components were rapid-prototyped from plastic (epoxy resin) material. Because plastic cannot be machined to very small thickness, the relative thickness of the UCI nozzle at the trailing edge is larger than that of the NATR nozzle. Figure 3 shows the combined stereolithography file of the three elements of the nozzle: fan nozzle, core nozzle, and plug.

The nozzle was attached to a dual-stream apparatus, shown in Fig. 4, that supplies mixtures of helium and air to the primary (core) and secondary (bypass) nozzles. The helium mass fraction and the total pressure p_0 of each mixture are determined by the desired exit velocity and Mach number. The nozzle size sets the individual mass flow rates of air and helium. Corresponding to the mass flow rate of air is the total pressure of the air flow alone, $p_{0_{\text{air}}}$. The helium mass fraction is set by first running air alone through the nozzle to match $p_{0_{\text{air}}}$, then adding helium to match p_0. This is the same procedure used by Doty and McLaughlin [6] in their single-stream, helium-air mixture jets. The total pressures were held to within 0.5% of the target values, resulting in errors of 0.4% in the velocity and 0.2% in the Mach number. Comparison of the UCI acoustic results with those from the NATR facility (which runs large-scale hot jets) shows excellent agreement in all measures of noise: spectal shapes, spectral levels, and overall sound pressure levels [5]. The exit flow conditions, listed in Table 1, matched the typical exit conditions of a turbofan engine with bypass ratio 4.8 at takeoff setting. The Reynolds number of the jet, based on fan diameter, was 0.6×10^6.

Noise Measurement

Noise measurements were conducted inside an anechoic chamber using a one-eighth inch condenser microphone (Brüel & Kjær 4138) with frequency response of 140 kHz. The microphone was mounted on a pivot arm and traced a circular arc centered at the jet exit with radius of $r = 0.96$ m. The polar angle θ ranged from 20° to 120° in intervals of 5° for $20° \leq \theta \leq 50°$ and 10° for the rest. Rotation of the nozzle assembly allowed variation of the azimuth emission angle. The azimuth angle typically took the values $\phi = 0°$, 30°, 60°, and 90°, although in some case only the angles $\phi = 0°$ and 60° were surveyed. The microphone was sampled at 400 kHz by a fast analog-to-digital board (National Instruments PCI-6070E) installed in a Pentium 4 computer. Each recording consisted of 54280 samples (135 ms), corresponding to the passage of about 10,000 eddies the size of the inner-jet diameter. The signal was high-pass filtered at 500 Hz by a Butterworth filter to remove spurious low-frequency noise. The narrowband power spectrum of the microphone voltage was computed using a 2048-point Fast Fourier Transform, which provided a spectral resolution of 195 Hz. The sound spectra were corrected for the microphone frequency response, free field response, and atmospheric absorption. Integration of the corrected spectrum yielded the overall sound pressure level (OASPL).

To predict full-scale noise perceived by a human observer, the sound spectra were extrapolated to frequencies higher than those resolved in the experiment (140 kHz) using a decay slope of -30 dB/decade. This was done to resolve the audible spectrum for a full-scale engine. The perceived noise level (PNL) results are very insensitive on the assumed slope. The spectra were then scaled up to engine size by dividing the laboratory frequencies by the appropriate scale factor.

PNL time histories and Effective Perceived Noise Levels (EPNLs) were computed for flyover and sideline monitors. The aircraft considered is twin-engine, each engine producing 90 kN of thrust (scale factor = 42). The flyover flight path is straight and level at an altitude of 460 m. The sideline noise is monitored on a line parallel to the runway centerline and offset by 450 m. In both cases, the aircraft velocity is 100 m/s ($M_\infty = 0.28$). The procedure for estimating PNL and EPNL has been described in earlier reports [3]. The full calculation for sideline EPNL is laborious and is based on the acoustic measurements at azimuth angles $\phi = 0°$, 30°, 60°, and 90°. It was determined, however, that a very accurate approximation of the sideline EPNL, to within 0.1 dB of the full calculation, can be obtained by combining the flyover EPNL values from the acoustic measurements at only $\phi = 0°$ and 60° as follows:

$$\text{EPNL}_{\text{sl}} = 0.15\ \text{EPNL}_{\text{fo},0} + 0.85\ \text{EPNL}_{\text{fo},60} - 2.2\ \text{dB}$$

In other words, the sideline EPNL is heavily influenced by sound emitted at $\phi = 60°$. To understand the meaning of $\text{EPNL}_{\text{fo},60}$, envision a flyover experiment where the airplane is flying straight and level but at a bank angle of 60°. This shortened procedure for estimating sideline EPNL expedites the experiments since only measurements at $\phi = 0°$ and 60° are required.

The reduction in cumulative EPNL (flyover plus sideline) is used here as a "figure of merit" for evaluating the noise reduction potential of FFD configurations. It does not necessarily correspond to the noise reduction from an actual airplane as this is influenced by many additional factors absent in our experiment (forward flight effect, engine installation effects, fan noise, etc). EPNL reductions are listed in Table 3 for each deflector configuration. The full calculation of sideline EPNL was performed for cases 4V and W_e, and the short calculation was done for cases W_i and 4V+W_e.

Deflectors

The deflector arrangements covered in this paper reflect an exploratory (not systematic) investigation of FFD in realistic-shaped nozzles. They are nor necessarily optimal. They encompass vane-type deflectors, wedge-type deflectors, and their combination. Table 2 describes the four configurations covered and Figs. 6-9 plot the corresponding geometries. The vanes were fabricated from thin (0.13-mm) brass sheet and were attached to the outer surface of the inner nozzle with adhesive. Electrical tape (0.18-mm thickness) was wrapped around the vanes to produce a round leading edge. The Mach numbers at the leading and trailing edges were estimated to be 0.4 and 0.7, respectively. The wedge deflectors were cut from 3.5-mm-thick nylon sheet. The height of the wedges matched the height of the fan duct at the nozzle exit.

It is evident from the diagrams of Figs. 6-9 that the 4V deflector is supposed to impart a mostly downward deflection of the bypass plume, while the wedge-type deflectors (external and internal) are expected to induce azimuthal motions that force the plume sideward (symmetrically around the vertical plane) and downward. The fluid mechanics of the wedge-type deflector are further discussed towards the end of this paper.

Acoustic Results

For each deflector configuration, and for microphone azimuth angles of 0° and 60°, we present spectra for several polar angles (plotted against full-scale frequency), OASPL directivities, and PNL time histories. Figure 10 shows the spectra of Case 4V. At $\theta = 20°$ we note a very deep reduction in the downward emission, reaching 17 dB at full-scale frequencies 200-500 Hz. Reduction in the sideline noise is moderate, approximately 5 dB at around 200 Hz. As the polar angle increases, the downward noise reduction remains substantial up to about $\theta = 60°$. The sideline reduction fades away for $\theta > 50°$. At $\theta = 90°$ the spectra of 4V practically coincide with those of the baseline jet. For higher angles, there is a slight increase in the spectral levels of 4V relative to the baseline.

The OASPL directivity for case 4V is shown in Fig. 11. We note substantial reductions in the downward OASPL for $\theta < 60°$ and in the sideline OASPL for $\theta < 40°$. Small increases in OASPL are noted for $\theta > 90°$. It is our experience that this "cross-over" in OASPL depends on the angle of attack of the vanes. As the angle of attack increases, the levels at low polar angles deepen dramatically but the levels in the forward arc increase. The sound increase at large θ, although moderate, can offset the PNL benefit of deep reductions at low θ. As a result, the EPNL benefit reaches a plateau beyond a certain vane angle of attack. This observation pertains to vane configurations having the overall geometry of case 4V. Other vane arrangements may not exhibit the same trend.

The flyover PNL histories for case 4V are shown in Fig. 12. Predictably, we note a large decrease in the downward PNL and a moderate decrease in the sideline PNL. The EPNL reductions are 4.3 dB for flyover and 1.9 dB for sideline. The cumulative reduction is a respectable 6.2 dB but, if sideline noise reduction is a priority, this arrangement may not be optimal. On the other hand, this is a very promising configuration for reducing the EPNL measured by the takeoff monitor.

We now examine the acoustics of the internal wedge deflector, case W_i. Figures 13 and 14 show some fundamental differences between the sound emission of W_i and those of vane arrangement 4V. First, the sound reductions in the downward and sideline directions are roughly the same. Second, reductions persist up to large polar angles, $\theta \approx 80°$. Third, there is very little crossover of OASPL at large θ. Even though the sound reduction at very low polar angles is not as dramatic as that of case 4V, the fact that significant sound reduction occurs over a large range of polar angles, combined with the little OASPL crossover for large θ, make this configuration acoustically superior to case 4V. This is evidenced by the PNL histories of Fig. 15 and the EPNL reductions of 4.5 dB flyover and 3.7 dB side-

line. The cumulative EPNL reduction of 8.2 dB is very substantial, especially considering how small this deflector is (Fig. 7). This EPNL estimate does not account for the small blockage in fan exit area, 3%, created on our nozzle (of course, if one were to implement this type of deflector on engine, the design of the fan duct would take the blockage into account). Considering the blockage, the cumulative EPNL reduction is 8.0 dB.

We now turn our attention to the external wedge deflector, case W_e. The obvious advantage of an external deflector is that it does not block the fan exit area. In fact, it may not require any redesign of the fan nacelle. In wing-mounted engines, the deflector could be part of the pylon structure. Figures 16-18 show that the acoustics of case W_e are very similar to those of case W_i. Sound reductions in the downward and sideline directions are practically equal. There is virtually no OASPL cross-over at large θ. We note sound reduction all the way up to $\theta = 100°$. The reduction in cumulative EPNL, 7.8 dB, is similar to that of case W_i and is evenly split in its flyover and sideline components.

The last configuration is the combination of cases 4V and W_e. The idea was to try to combine the best attributes of the vane-type deflector (deep reductions of downward sound at low θ) with those of of the wedge-type deflector (reductions over large range of θ, good sideline suppression, little or no OASPL cross over in the forward arc). Figures 19-21 show that the combination is indeed successful. Sound in the downward direction is noticeably lower that than of W_e, while sound in the sideline direction is about the same as that of W_e. The EPNL reductions are 5.5 dB for flyover and 3.8 dB for sideline. The cumulative EPNL is reduced by 9.2 dB.

Discussion

The noise reduction characteristics of case 4V (Figs. 10-12) are consistent our basic model of FFD, namely the reduction in convective Mach number and resultant attenuation of sound generated by large-scale turbulent structures. In jets with low to moderate speeds, sound from large-scale structures dominates the downstream direction.

The wedge-type deflectors suppress sound not only near the jet axis but also at polar angles up to $\theta = 100°$. Our current understanding of jet noise is that sound at large angles is dominated by noise generated by fine-scale turbulence [7]. It is possible, therefore, that we are dealing with an additional type of noise suppression that is not captured by the current model of FFD. It may have to do with refraction of fine-scale noise, reshaping of the core plume, and possibly other factors. It is hoped that some answers will come from a study of the mean flow field, which is currently underway.

The aerodynamics of the wedge-type deflector are intriguing and will be the subject of computational and experimental studies. It is important to note we are dealing with a situation very different from the classical flow around a wedge. The difference lies in the fact that the outward face and the base of the wedge are exposed to ambient air. Therefore, the base does not need to be "filled" by the fluid flowing around the edges of the wedge. In other words, the streamlines originating from the corners of the base are expected to diverge and not form a recirculation region. Absence of a recirculation region means that the drag of the wedge is very low, much lower than that of the classical problem.

Crude surface flow visualizations, conducted in a series of experiments, support the above arguments. A blob of ink was placed upstream of the wedge and the bypass stream was turned on. A typical streak pattern with external wedge is shown in Fig. 22. Downstream of the wedge, the steaklines maintain the general direction imparted to them by the angle of the wedge. There is no sign at all of a recirculating region. Further evidence for the absence of a recirculation region is the noise reduction itself. If the streamlines "closed" behind the wedge, the net flow deflection would be zero and it would be very difficult to explain the noise reductions measured here.

At forward flight, the wedge will develop a wake behind it because of the flow of ambient air over the backward-facing step (base) of the wedge. The drag of the wedge will be similar to that of the classical wedge problem with a freestream Mach number equal to the flight Mach number. The practical implementation of this device is active, i.e., it will be deployed during the noise-sensitive segments of flight (takeoff and possibly landing) and stowed otherwise. During takeoff/landing the airplane is "dirty" anyway, so the external drag of the wedge should have minimal impact on performance.

Conclusion

We have shown that fan flow deflectors implemented on realistic nozzles can produce substantial noise suppression. The noise reduction achieved by the particular vane-type deflector tested here was strong in the downward direction and moderate in the sideline direction. Wedge-type deflectors generated significant attenuation in both the downward and sideline noise emissions. Combination of vanes and wedge yielded the best noise reduction. The effective perceived noise level was suppressed by 5.5 dB in flyover mode and 3.8 dB in sideline mode. The measurements suggest reduction not only of the noise generated by large-scale structures, but also of noise caused by fine-scale turbulence.

Acknowledgments

The support by NASA Glenn Research Center is gratefully acknowledged (Grant NAG-3-2345 monitored by Dr. Khairul B. Zaman and Dr. James Bridges). Dr. Bridges is especially thanked for providing us with the NATR nozzle coordinates. The method and system of noise suppression via deflection of the bypass and/or core streams is proprietary to the University of California. U.S. Patent Pending.

References

[1] Saiyed, N.H., Mikkelsen, K.L., and Bridges, J.E., "Acoustics and Thrust of Separate-Flow High-Bypass-Ratio Engines," *AIAA Journal*, Vol. 41, No. 3, 2003, pp. 372-378.

[2] Papamoschou, D. "Mean Flow and Acoustics of Dual-Stream Jets," AIAA-2004-0004.

[3] Papamoschou, D. and Nishi, K.A., "Turbofan Jet Noise Reduction via Deflection of the Bypass Streem," AIAA-2004-0187.

[4] Janardan, B.A., Hoff, G.E., Barter, J.W., Martens, S., Gliebe, P.R., Mengle, V., and Dalton, W.N., "AST Critical Propulsion and Noise Reduction Technologies for Future Commercial Subsonic Engines Separate-Flow Exhaust System Noise Reduction Concept Evaluation," NASA CR 2000-210039.

[5] Papamoschou, D. "Acoustic Simulation of Hot Coaxial Jets using Cold Helium-Air Mixture Jets," AIAA-2005-0208.

[6] Doty, M.J. and McLaughlin, D.K., "Acoustic and Mean Flow Measurements of High-Speed, Helium-Air Jets," *International Journal of Aeroasouctics,* Vol. 2, No. 3 & 4, 2003, pp.293-333.

[7] Tam, C.K.W., "Jet Noise: Since 1952," *Theoretical and Computational Fluid Dynamics,*" Vol. 10, 1998, pp. 393-405.

Table 1 Exit flow conditions

Quantity	Core	Fan
Nozzle diameter (mm)	17.0	31.0
Plug diameter (mm)	11.5	-
Height of exit annulus (mm)	2.2	3.1
Lip thickness (mm)	0.8	0.8
Velocity (m/s)	460	334
Mach number	0.86	0.95
Bypass ratio	-	4.8

Table 2 Deflector Configurations

Case	Configuration
Base	Clean nozzle
4V	Two pairs of vanes at ϕ=70° and ϕ=110°, $\alpha = 10°$, c=4 mm, $x_{te} = -1$ mm.
W_i	Internal wedge with $\alpha = 17°$, $\ell = 5$ mm.
W_e	External wedge with $\alpha = 18°$, $\ell = 10$ mm.
4V+W_e	Combination of 4V with W_e.

α = angle of attack for vane, half-angle for wedge
c = chord length of vane airfoil
ℓ = length of side of wedge
ϕ= azimuth angle measured from the downward vertical direction
x_{te} = axial location of trailing edge relative to exit of fan nozzle

Table 3 EPNL Reduction (dB)

Case	Flyover	Sideline	Cumulative
4V	4.3	1.9	6.2
W_i	4.5	3.7	8.2
W_e	4.0	3.9	7.9
4V+W_e	5.5	3.8	9.2

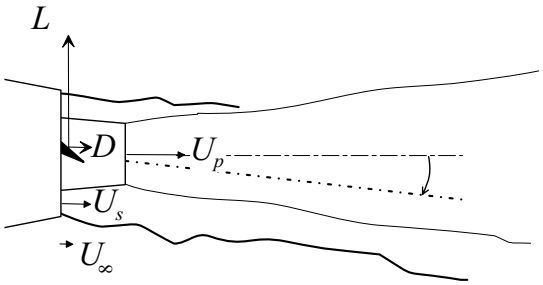

Fig.1 General concept of Fan Flow Deflection (FFD).

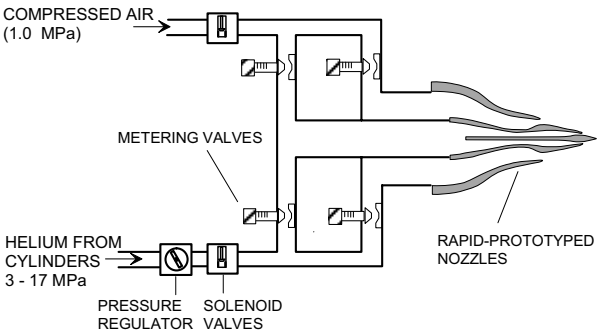

Fig.4 Dual-stream jet apparatus.

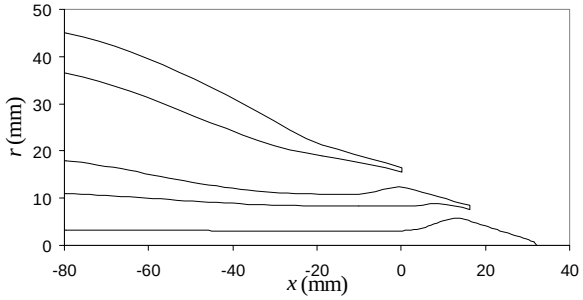

Fig.2 Radial coordinates of UCI nozzle.

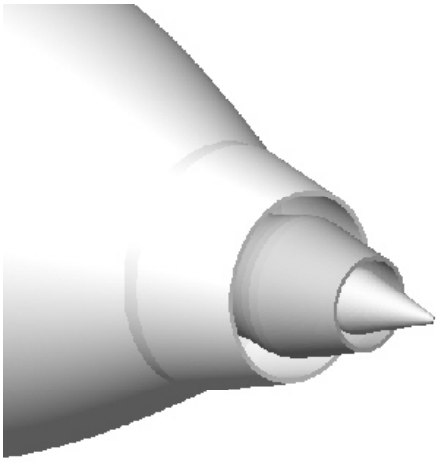

Fig.3 Stereolithography grid of UCI nozzle.

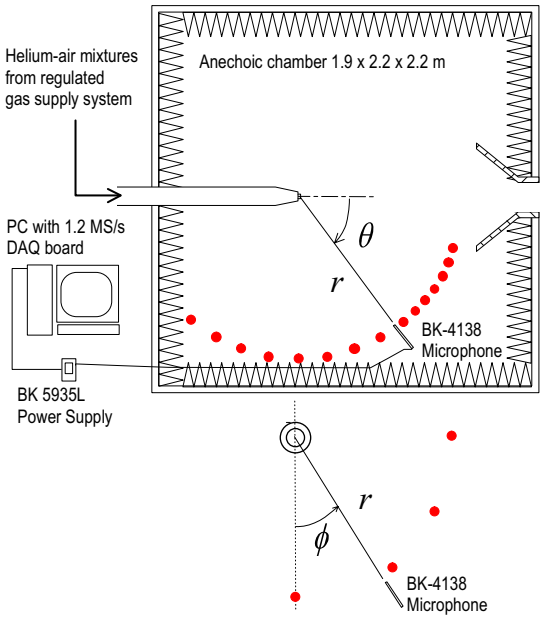

Fig.5 UCI Jet Aeroacoustics Facility.

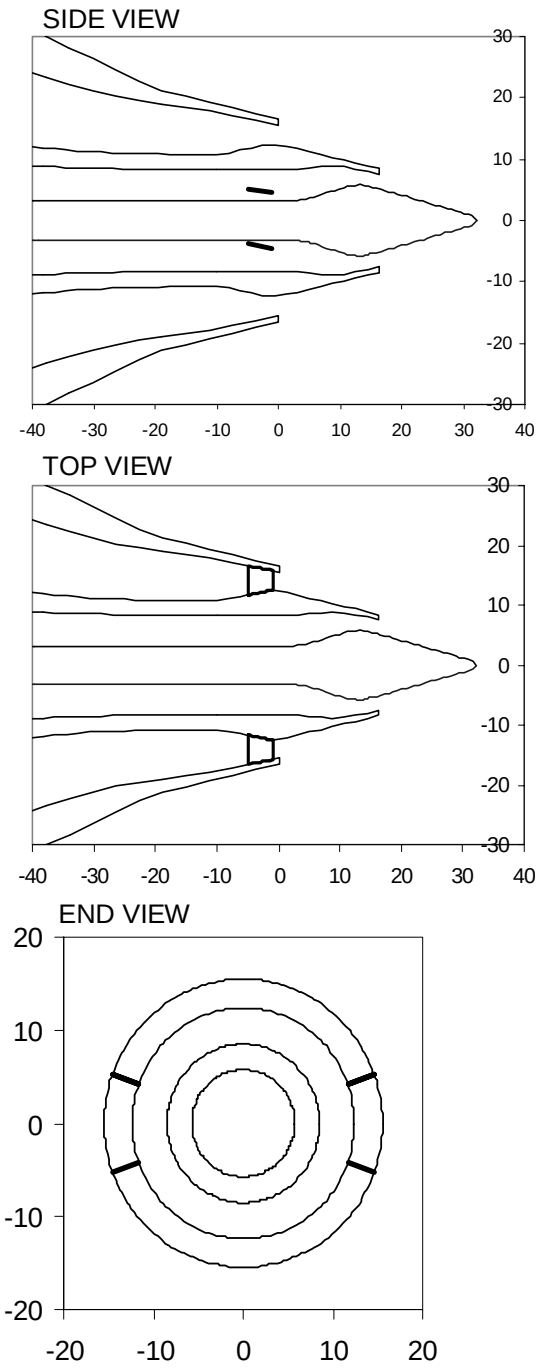

Fig.6 Deflector configuration with two pairs of vanes (4V).

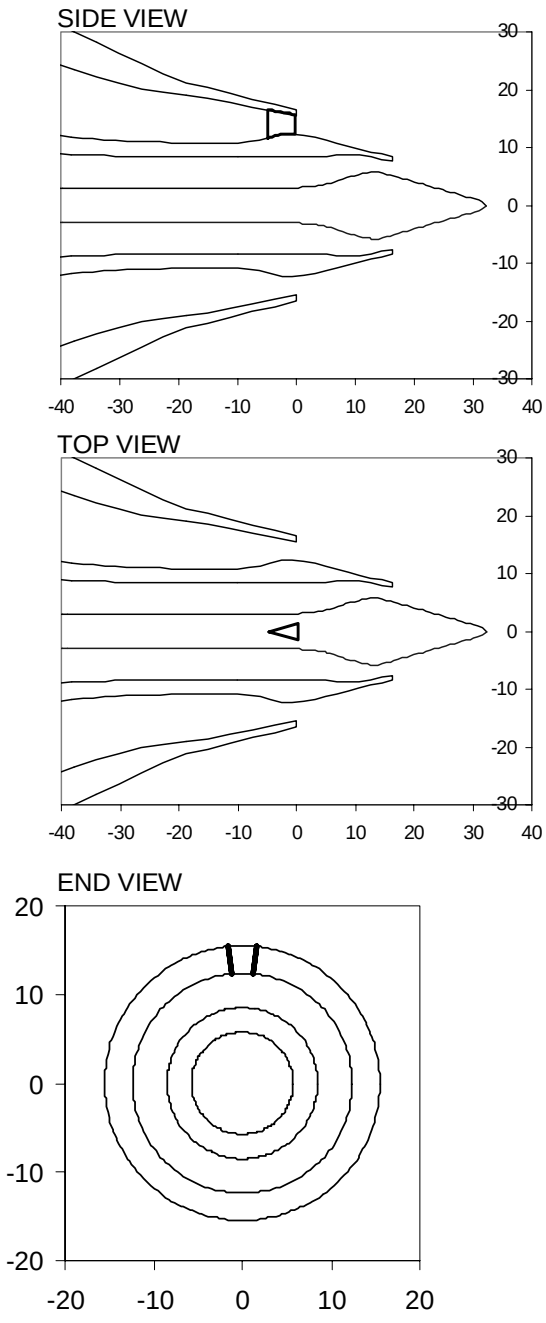

Fig.7 Deflector configuration with internal wedge (W_i).

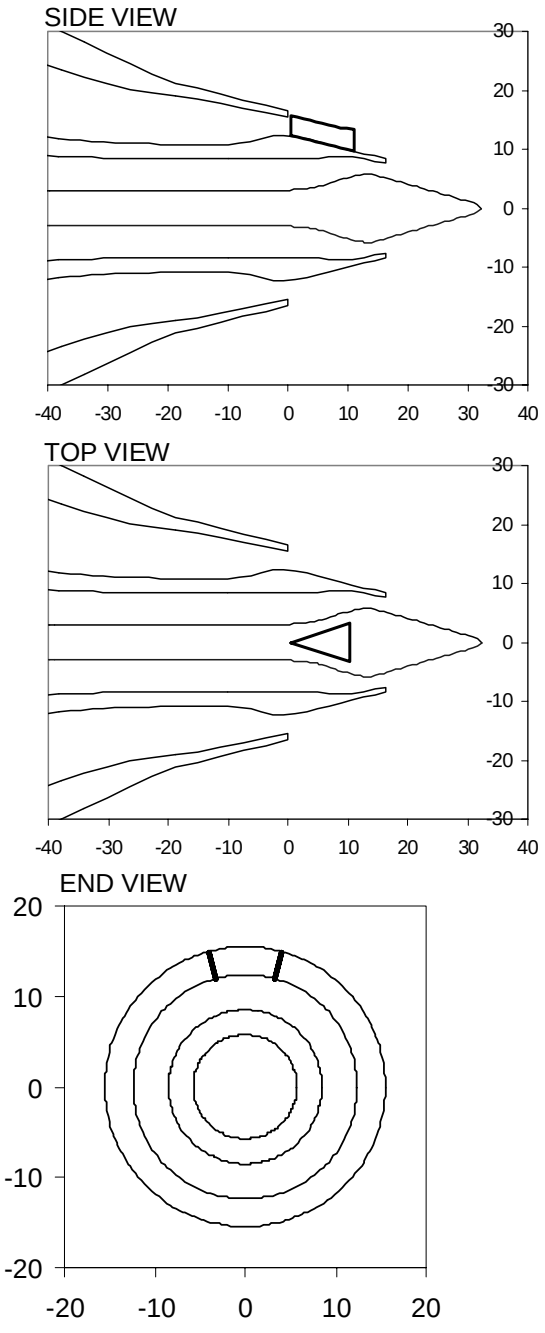

Fig.8 Deflector configuration with external wedge ($\mathbf{W_e}$).

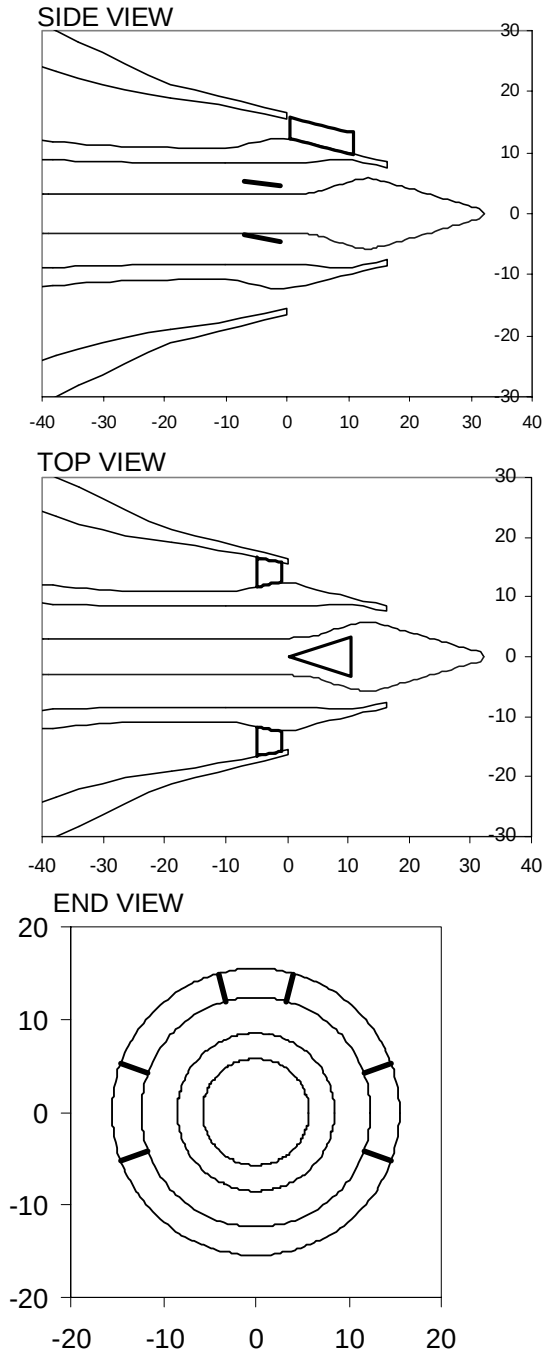

Fig.9 Deflector configuration with two pairs of vanes and external wedge ($\mathbf{4V+W_e}$).

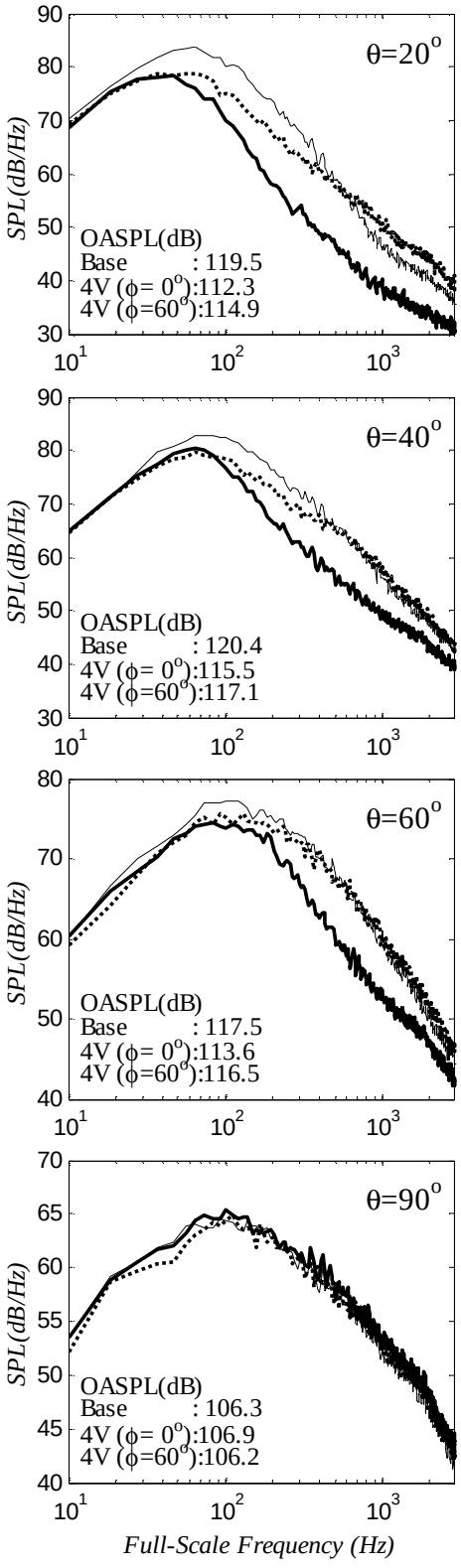

Fig.10 Far field spectra for case 4V at various polar angles. Thin line: baseline; thick lines: 4V at microphone azimuth angles 0° (solid) and 60° (dotted).

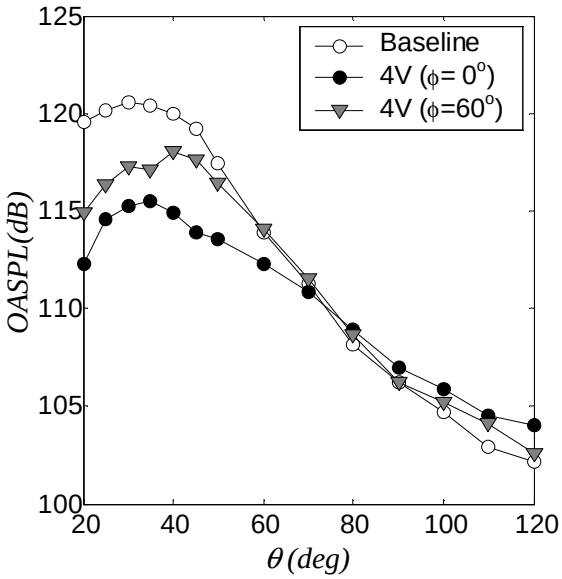

Fig.11 Overall sound pressure levels for case 4V at microphone azimuth angles 0° and 60°.

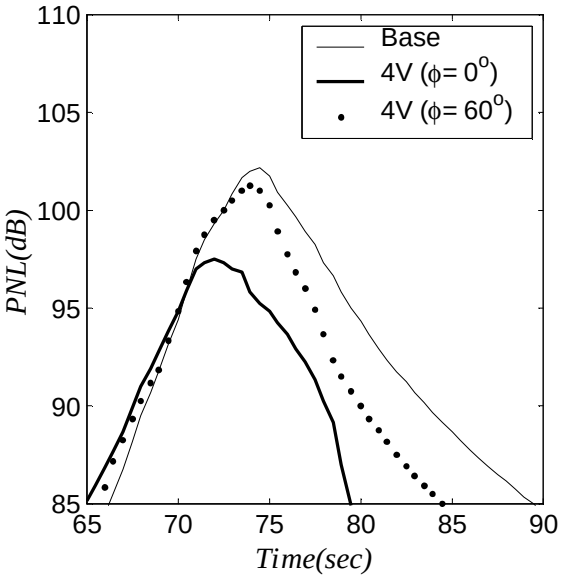

Fig.12 Flyover perceived noise level history for case 4V based on microphone azimuth angles 0° and 60°.

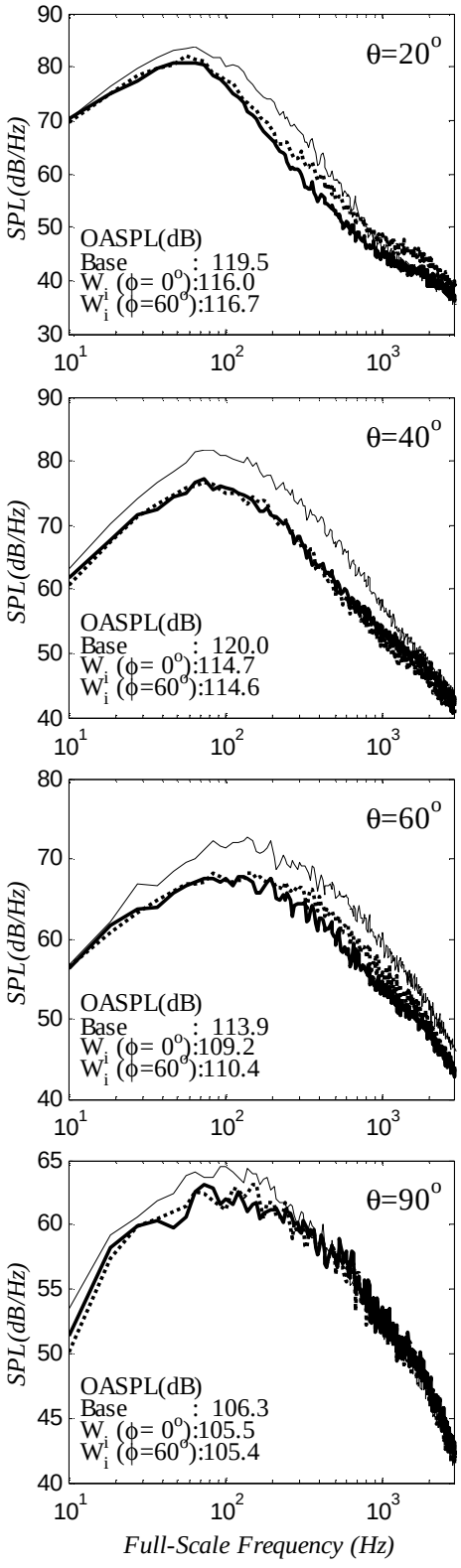

Fig.13 Far field spectra for case W_i at various polar angles. Thin line: baseline; thick lines: W_i at microphone azimuth angles 0° (solid) and 60° (dotted).

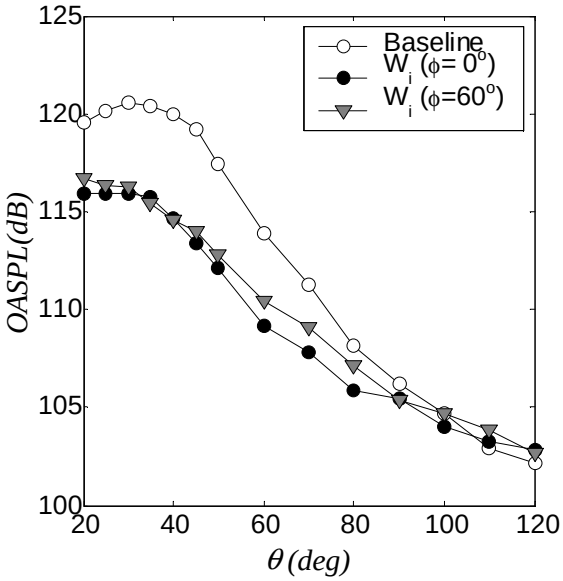

Fig.14 Overall sound pressure levels for case W_i at microphone azimuth angles 0° and 60°.

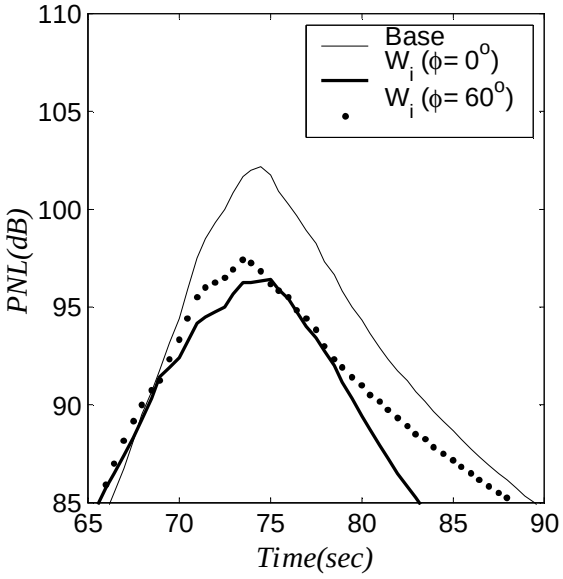

Fig.15 Flyover perceived noise level history for case W_i based on microphone azimuth angles 0° and 60°.

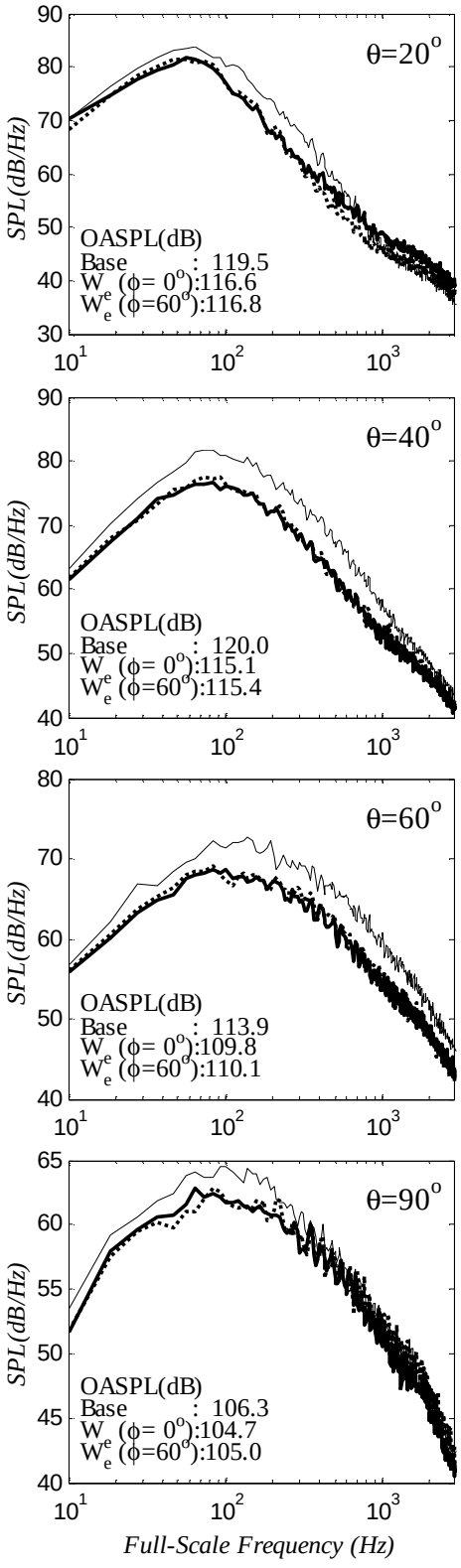

Fig.16 Far field spectra for case W_e at various polar angles. Thin line: baseline; thick lines: W_e at microphone azimuth angles 0° (solid) and 60° (dotted).

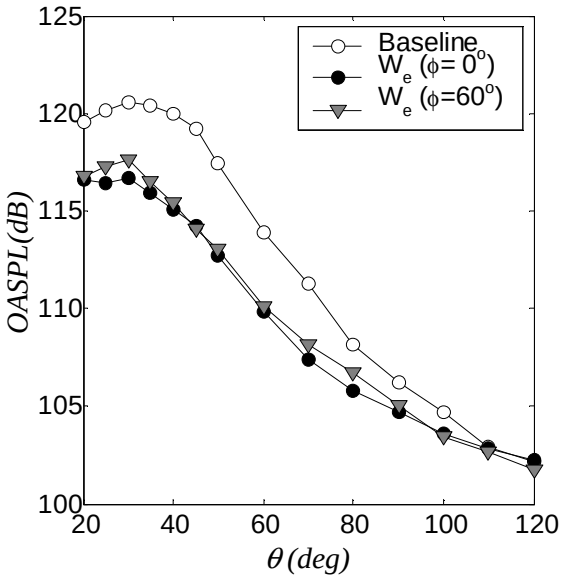

Fig.17 Overall sound pressure levels for case W_e at microphone azimuth angles 0° and 60°.

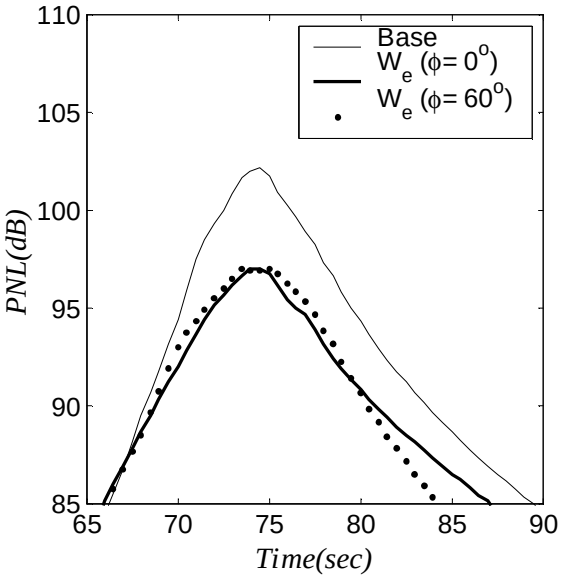

Fig.18 Flyover perceived noise level history for case W_e based on microphone azimuth angles 0° and 60°.

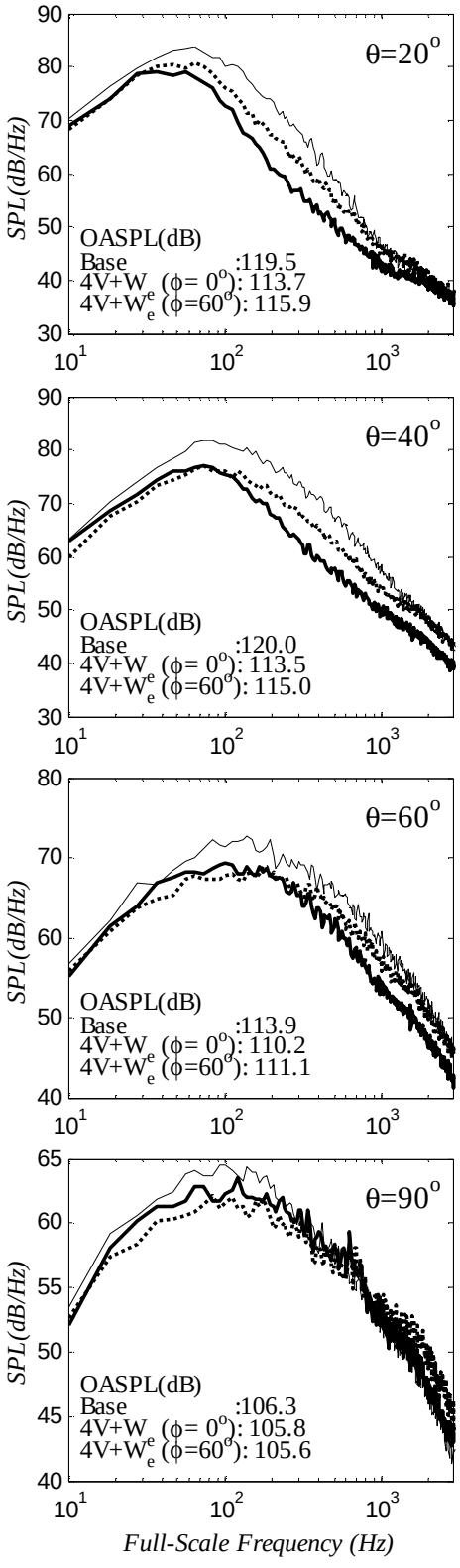

Fig.19 Far field spectra for case 4V+W_e at various polar angles. Thin line: baseline; thick lines: 4V+W_e at microphone azimuth angles 0° (solid) and 60° (dotted).

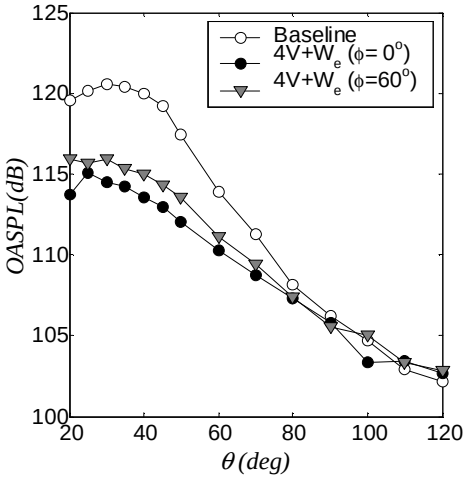

Fig.20 Overall sound pressure levels for case 4V+W_e at microphone azimuth angles 0° and 60°.

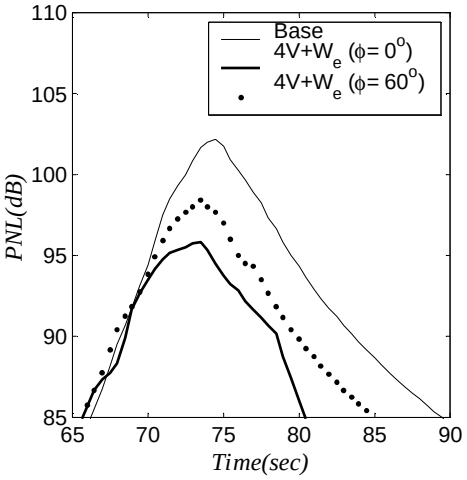

Fig.21 Flyover perceived noise level history for case 4V+W_e based on microphone azimuth angles 0° and 60°.

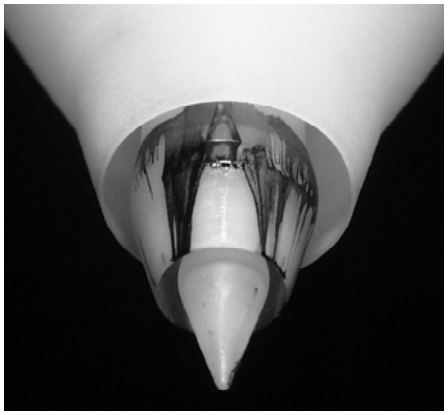

Fig.22 Surface visualization of flow around external wedge.